

Enhanced Oxygen Electrocatalysis in Heterostructured Ceria Electrolytes for Intermediate-Temperature Solid Oxide Fuel Cells

Tao Hong,^{*,†,‡,§} Yanxiang Zhang,[§] and Kyle Brinkman^{*,†,‡,||}

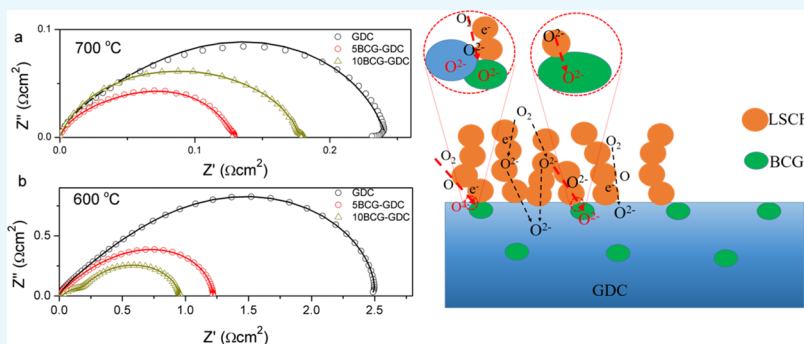
[†]School of Materials Science and Engineering, Hefei University of Technology, Tunxi Road 193, Hefei 230009, China

[‡]Department of Materials Science and Engineering, Clemson University, Clemson, South Carolina 29634, United States

[§]National Key Laboratory for Precision Hot Processing of Metals, School of Materials Science and Engineering, Harbin Institute of Technology, Harbin 150001, China

^{||}U.S. Department of Energy, National Energy Technology Laboratory, 3610 Collins Ferry Rd, P.O. Box 880, Morgantown, West Virginia 26507-0880, United States

Supporting Information



ABSTRACT: Heterostructured composite ceria electrolytes have been shown to accelerate the oxygen reduction activity and provide a new approach to improve solid oxide fuel cell (SOFC) performance. In this study, barium carbonate was added to gadolinium-doped ceria, $\text{Gd}_{0.2}\text{Ce}_{0.8}\text{O}_{2-\delta}$ (GDC) electrolyte to improve the electrochemical performance of intermediate-temperature SOFCs. The heterostructured electrolyte was formed by the addition of 5 wt % BaCO_3 to a GDC electrolyte, resulting in a reaction during sintering that formed well-dispersed $\text{BaCe}_{0.8}\text{Gd}_{0.2}\text{O}_{3-\delta}$ (BCG) throughout the electrolyte. The resulting material was tested as an electrolyte using $\text{La}_{0.6}\text{Sr}_{0.4}\text{Co}_{0.2}\text{Fe}_{0.8}\text{O}_{3-\delta}$ as a cathode, resulting in a dramatic reduction to the polarization resistance of more than half the value (600 and 700 °C, the resistance was reduced from 2.49 and 0.23 $\Omega \text{ cm}^2$ to 1.21 and 0.12 $\Omega \text{ cm}^2$) obtained by using pure GDC as an electrolyte. Furthermore, full cell SOFC tests employing the heterostructured electrolyte conducted during overextended durations indicated that the BCG phase in the 5BCG–GDC electrolyte was stable in an air atmosphere with no observed reactions with residual CO_2 . This approach of tailoring surface reactivity by tailoring the composition and structure of the electrolyte as opposed to electrode materials provides an alternative method to improve fuel cell performance.

INTRODUCTION

Ceria (CeO_2)-based materials have attracted extensive attention because of their potential use as an intermediate temperature electrolyte for solid oxide fuel cells (SOFCs).^{1–7} The interest in this material is due to the enhanced ionic conductivity of doped ceria electrolytes as compared to conventional oxygen ion conducting electrolytes based on yttria-stabilized zirconia. Despite the promising ionic conduction properties of CeO_2 -based electrolytes, their use is limited by reduction of Ce at low oxygen partial pressure, which results in electronic conductivity and a decreased open circuit potential. Attempts to optimize the functional properties of doped ceria electrolytes have relied on two principal strategies: (i) bilayer electrolytes fabricated via sputtering or sol–gel coating process to block electric conduction and (ii)

through the creation of composite materials based on cerium oxide and barium. Bilayered electrolyte membranes composed of $\text{BaZr}_{0.1}\text{Ce}_{0.7}\text{Y}_{0.2}\text{O}_{3-\delta}$ (BZCY) and $\text{Ce}_{0.8}\text{Sm}_{0.2}\text{O}_{2-\delta}$ (SDC) have been explored for use in SOFCs and the results of electrochemical testing indicated the electron-blocking ability of the BZCY layer in the fuel cell. Prior work on composite systems has focused on a few material combinations such as $\text{BaCe}_{0.8}\text{Y}_{0.2}\text{O}_{3-\delta}$ – $\text{Ce}_{0.8}\text{Gd}_{0.2}\text{O}_{1.9}$, $\text{BaCe}_{0.8}\text{Y}_{0.2}\text{O}_{3-\delta}$ –SDC, and $\text{BaCe}_{0.8}\text{Sm}_{0.2}\text{O}_{3-\delta}$ (BCS)–SDC. It was demonstrated that the double-matrix structure of BCS–SDC (weight ratio 1:1) could avoid the typical drawbacks of doped ceria electrolytes. In

Received: August 22, 2018

Accepted: October 9, 2018

Published: October 18, 2018

addition to material combinations listed above employing oxide ionic conductors, acceptor-doped BaCeO_3 , which is a mixed proton and oxygen ion conductor, has demonstrated the ability to block electronic conduction and protect doped ceria from reduction.^{8,9} It was found that the electron-blocking ability of the composite was highly dependent on the amount of BaCeO_3 and increased with increasing BaCeO_3 content.

The function of the cathode in SOFCs is to provide reaction sites to reduce oxygen molecules to oxygen anions; this reaction typically has a high activation energy and dominates overall performance characteristics of SOFCs. A significant number of cathode materials have been evaluated on doped ceria electrolytes, including perovskite-type $\text{La}_{1-x}\text{Sr}_x\text{MnO}_{3-\delta}$,¹⁰ $\text{La}_{1-x}\text{Sr}_x\text{Co}_{1-y}\text{Fe}_y\text{O}_{3-\delta}$,¹¹ $\text{Ba}_{0.5}\text{Sr}_{0.5}\text{Co}_{0.8}\text{Fe}_{0.2}\text{O}_{3-\delta}$ layered double perovskite,¹³ as well as Ruddlesden–Popper-type materials.^{14,15} Although some of these cathode materials show high oxygen reduction reaction (ORR) activity at intermediate temperatures, the performance has not been fully optimized. As a result, extensive contemporary efforts have been devoted to developing new catalyst materials with varied infiltration approaches to enhance the performance of existing SOFC cathodes and evaluate their long-term durability.^{16–18}

Prior works on composite electrolytes have focused on ionic conductivity contributions at the interface because of redistribution of ions in the space-charge regions.^{19–22} However, the effect of a heterostructured electrolyte on the cathode electrochemical performance has not been reported to date. In this work, we report a novel method to improve the cathode performance by the formation of a well-dispersed barium cerate phase in a doped ceria electrolyte. The resulting material was tested as an electrolyte using $\text{La}_{0.6}\text{Sr}_{0.4}\text{Co}_{0.2}\text{Fe}_{0.8}\text{O}_{3-\delta}$ (LSCF) as a cathode, resulting in a dramatic reduction to the polarization resistance of more than half the value (600 and 700 °C, the resistance was reduced from 2.49 and 0.23 to 1.21 and 0.12 $\Omega \text{ cm}^2$) obtained by using pure $\text{Gd}_{0.2}\text{Ce}_{0.8}\text{O}_{2-\delta}$ (GDC) as an electrolyte. In addition, the heterostructured ceria electrolyte exhibited good long-term stability in full cell operating conditions.

RESULTS AND DISCUSSION

BCG Phase Formation and Sintering Behavior. Figure 1a–c shows the X-ray diffraction (XRD) patterns for a pure GDC pellet sintered at 1500 °C exhibiting the fluorite structure. However, when mixed with 5 or 10 wt % BaCO_3 and sintered at 1500 °C for 5 h, additional peaks appear in the spectra, which are consistent with a BaCeO_3 -based perovskite structure. Additional details of the reaction process were sought at a higher BaCO_3 mixture content. Figure 1d–i shows the XRD spectra of GDC/ BaCO_3 mixed in an 88.14:100 weight ratio (50:50 in mol ratio) at temperatures from 800 to 1500 °C. A reaction initiates at temperatures near 1000 °C, whereas below 900 °C the materials retain their original structure. Although bulk phases have not been synthesized and characterized, it has been reported that Ba vapor could react with doped ceria electrolytes to form a Ba cerate thin film.^{23,24} This work extends the solid–vapor reaction data to bulk reactions, indicating that a perovskite phase of the $\text{BaCe}_{0.8}\text{Gd}_{0.2}\text{O}_{3-\delta}$ (BCG) forms during the sintering process according to $(\text{Gd}_{0.2}\text{Ce}_{0.8}\text{O}_{2-\delta} + \text{BaCO}_3 \rightarrow \text{BCG} + \text{CO}_2)$. The resulting heterostructured electrolyte retains the original phase assemblage after extended heat treatments at 1500 °C as shown in Figure 1d.

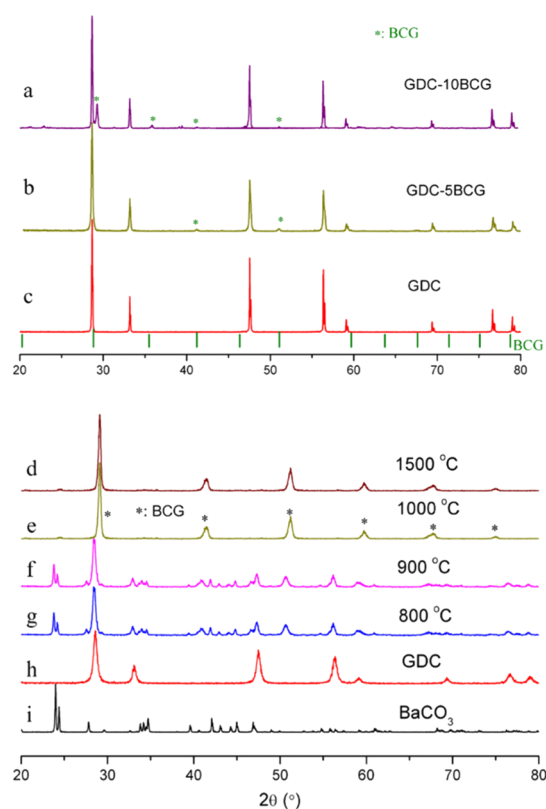


Figure 1. XRD patterns for (a) 10BCG–GDC (10% BaCO_3), (b) 5BCG–GDC (5% BaCO_3), and (c) pure GDC pellets sintered at 1500 °C for 5 h. GDC– BaCO_3 composite powder (mole ratio of 50:50) calcined at (d–g) 1500, 1000, 900, and 800 °C respectively, (h) pure GDC powder, and (i) pure BaCO_3 powder.

The reaction processes between BaCO_3 and GDC were investigated using thermal gravitational measurement by recording the weight change during the heating process. As shown in Figure 2a, the weight loss of GDC from 30 to 1500 °C was about 3.5%. In contrast, the weight loss for GDC with 5 wt % BaCO_3 was close to 5%. The higher weight loss of BaCO_3 –GDC is due to the additional weight loss of CO_2 , $44.01/197.35 \times 5\% = 1.16\%$. Another important factor for processing GDC and BaCO_3 –GDC composites is the sintering behavior. The sintering curves of GDC and GDC with 5 wt % BaCO_3 are shown in Figure 2b. It is seen that both materials have similar sintering activity, exhibiting a relative density increase at 800 °C with complete densification near 100% density achieved at temperatures near 1500 °C. Scanning electron microscopy (SEM) images for GDC and 5BCG–GDC are shown in Figure 2c–d, and energy dispersive X-ray (EDX) mapping images for Ce, Gd, and O are presented in Figure S1. It was found that the materials were fully dense and that the grain size was enhanced by BaCO_3 addition. The mean grain size of 5BCG–GDC was 0.5 μm , whereas it was 3.46 times larger at 2.23 μm for 5BCG–GDC. The enhanced grain growth may be due to evolved CO_2 at 1000 °C during the sintering process in the 5BCG–GDC samples.

Ionic Conductivity of GDC and 5/10BCG–GDC Electrolytes. The ionic conductivities of GDC, 5BCG–GDC, and 10BCG–GDC are shown in Figure 3a. At 600 °C, the conductivity of GDC was 0.029 S cm^{-1} , which is consistent with the reported value.^{2,25} The conductivity decreased to 0.025 S cm^{-1} for 5BCG–GDC and further to 0.021 S cm^{-1} for

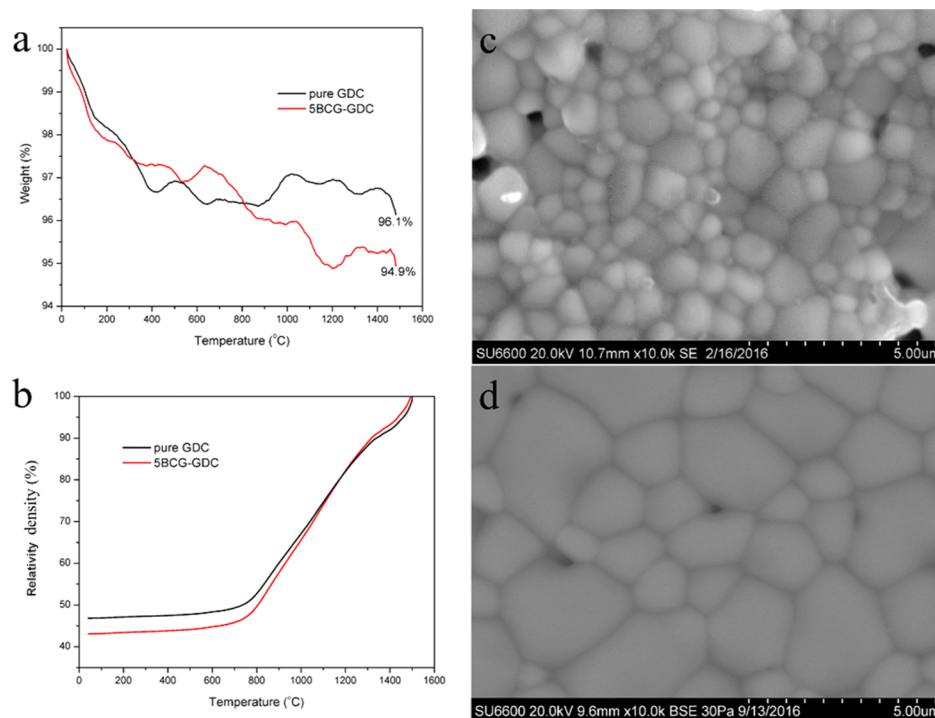


Figure 2. SEM image of the surface and cross section for (a,b) pure GDC and (c,d) GDC-Ba electrolytes sintered at 1500 °C for 5 h.

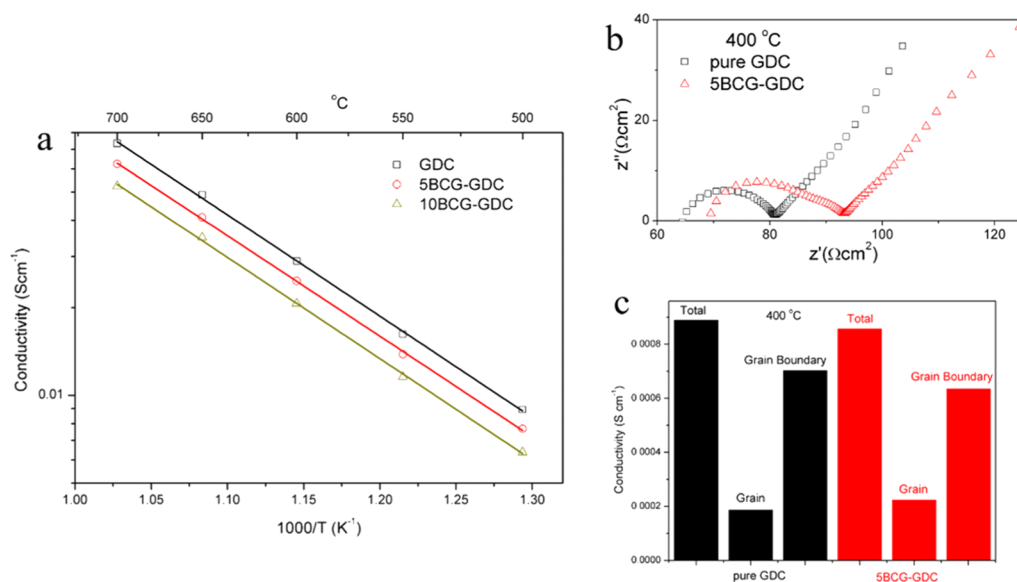


Figure 3. (a) Ionic conductivity of pure GDC, 5BCG–GDC, and 10BCG–GDC electrolytes, (b) impedance spectra, and (c) contribution of grain and grain-boundary conductivity at 400 °C.

10BCG–GDC. Over the temperature range from 500 to 700 °C, the samples exhibit the same trend. Literature values for the oxygen ionic conductivity of BCG are 0.012 and 0.023 S cm⁻¹ at 600 and 700 °C,^{26–28} respectively, which are much lower than those of GDC. Therefore, the reduction in conductivity of composite 5BCG–GDC samples may be due to increased BCG content. The grain conductivity and grain boundary conductivity were examined from fits of the impedance spectra at 400 °C as shown in Figure 3b. At 400 °C, the grain and grain boundary conductivity of GDC was 1.87×10^{-4} and 7.02×10^{-4} S cm⁻¹, respectively. For the 5BCG–GDC sample, the values were 2.23×10^{-4} and 6.35×10^{-4} S cm⁻¹ as shown in Figure 3c. The decrease of grain

boundary conductivity in heterostructured samples may be attributed to the nature of the interface between GDC and BCG and the increased grain size resulting in less interfacial contributions.

LSCF Cathode Performance in GDC and 5/10BCG–GDC Electrolytes. The conductivity experiments outlined above indicated only a slight decrease in the level of oxygen ion conductivity in 5BCG–GDC and 10BCG–GDC as compared to the baseline GDC electrolyte. In order to examine the polarization resistance properties of interest for fuel cell applications, an LSCF cathode was used to fabricate and test symmetrical cells. Figure 4 summarizes the effect of the BCG phase in the GDC electrolyte on the LSCF electrode area

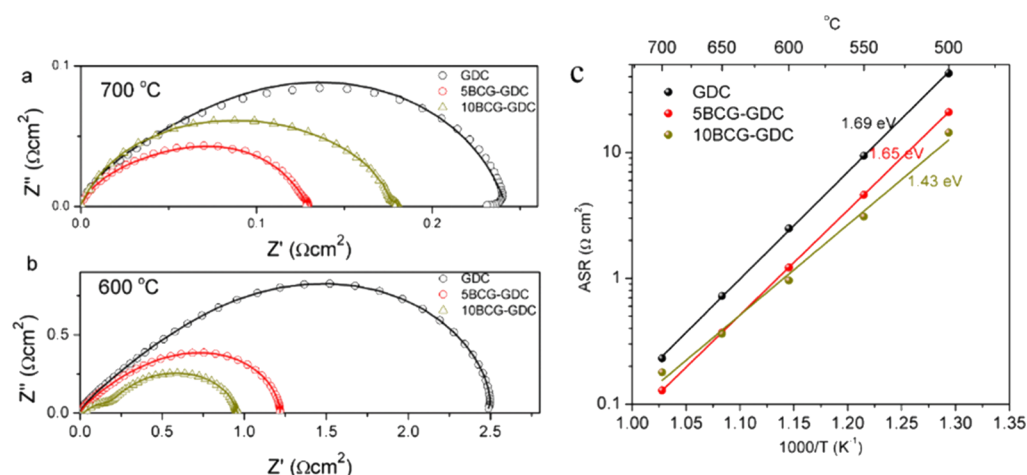


Figure 4. (a,b) Impedance spectra of the LSCF cathode in GDC, 5BCG–GDC, and 10BCG–GDC electrolytes at 700 and 600 °C and (c) area specific polarization resistance (ASR) of the LSCF electrode on GDC, 5BCG–GDC, and 10BCG–GDC from 500 to 700 °C.

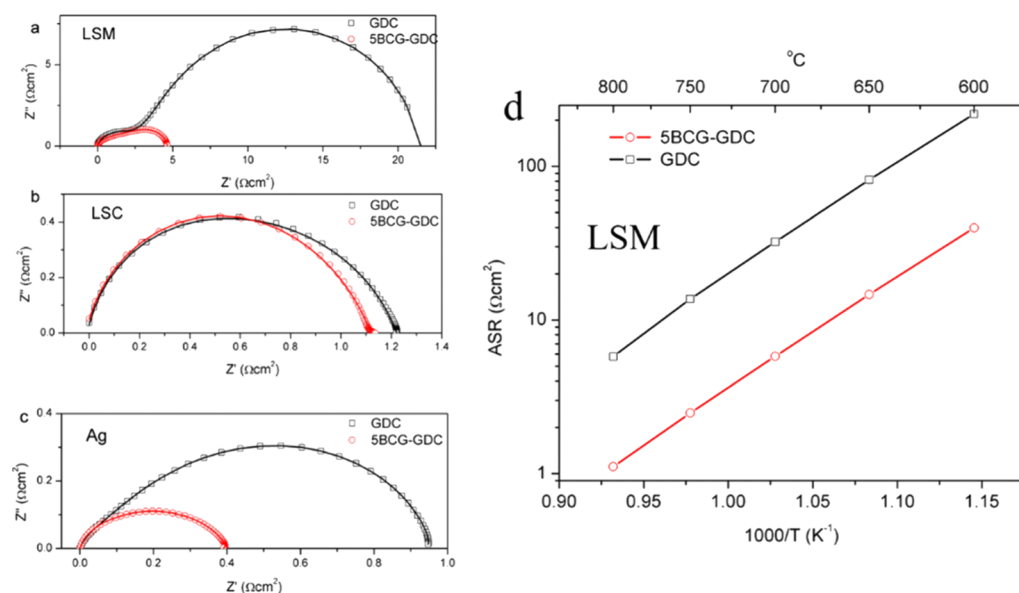


Figure 5. Polarization resistance of (a) LSM, (b) LSC, and (c) Ag on GDC and 5BCG–GDC electrolytes at 700 °C and (d) corresponding ASR value of the LSM electrode from 600 to 800 °C.

specific resistance (ASR), which is determined from the ac impedance spectra. Figure S2 displays the cross section of the LSCF electrode on all electrolytes, which shows a similar morphology. The resistance of the LSCF electrode in 5BCG–GDC and 10BCG–GDC electrolytes was found to be half the value of that of LSCF/GDC electrolytes. For example, at 700 and 600 °C (Figure 4a,b), the LSCF electrode exhibits an ASR of 0.23 and 2.5 $\Omega \text{ cm}^2$ on pure GDC electrolytes, which is consistent with previously reported values.^{29,30} The values observed in this work were 0.13, 1.21 and 0.18, 0.96 $\Omega \text{ cm}^2$ on 5BCG–GDC and 10BCG–GDC electrolytes, respectively. Bode plots (Figure S3) indicate that the reduced resistance is attributed to greatly reduced low-frequency resistance (around 10 Hz at 600 °C) that is associated with charge transfer from the LSCF electrode to the electrolyte.^{31–33} Figure 4c displays the activation energy which was observed to decrease from 1.69 eV in GDC to 1.65 eV in 5BCG–GDC and further to 1.43 eV in the 10BCG–GDC electrolyte system.

A comparison of the heterostructured electrolytes indicate that the 5BCG–GDC electrolyte was more suitable for

application in full cell SOFC because of the higher ionic conductivity and smaller polarization resistance. In further work, $\text{La}_{0.8}\text{Sr}_{0.2}\text{MnO}_{3-\delta}$ (LSM), LSC, and Ag were also employed to evaluate the cathode performance on GDC and 5BCG–GDC electrolytes. These three materials stand for electronic conductor, mixed conductor, and precious metal as cathode. Figure 5a–c shows the typical impedance spectra measured at 700 °C with symmetrical cells for LSM, LSC, and Ag electrodes. At 700 °C, the area specific resistance (ASR) shows that the ASR of LSM, LSC, and Ag on GDC was 20.6, 1.22, and 0.95 $\Omega \text{ cm}^2$, whereas it was 4.6, 1.13, and 0.39 $\Omega \text{ cm}^2$ in 5BCG–GDC, respectively. The morphology of all three electrodes on GDC and 5BCG–GDC electrolytes is shown in Figure S2. The ASR value for the LSM electrode exhibited the greatest decrease on 5BCG–GDC electrolytes as shown in Figure 5d. However, all the cathodes utilized exhibited improved cathode performance when using the 5BCG–GDC electrolyte as compared to pure GDC.

3D Microstructure of 5BCG–GDC Electrolytes. The SEM–EDX spectroscopy images of GDC and 5BCG–GDC

are shown in Figure 6a. In the cross section, we can find that the Ba elemental edge in the EDX-mapping is evenly

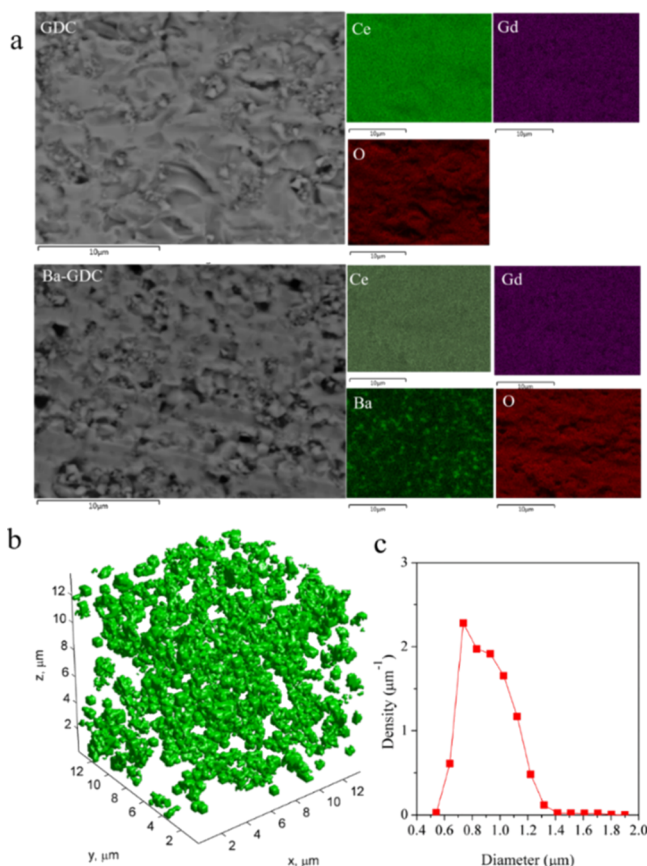


Figure 6. (a) SEM–EDX images for GDC and SBCG–GDC electrolytes, (b) 3D distribution image of the BCG phase in the GDC matrix, and (c) grain size distribution of the BCG phase.

distributed throughout the cross section. On the basis of the observed the Ba elemental distribution and the amount of BaCO₃ added as weight percent in the matrix (volume fraction 6.25%), it appears that the BCG phase is evenly distributed throughout the bulk of the material. In the heterostructured electrolyte, the BCG phase appears as isolated grains as shown in Figure 6b. The BCG grain size ranged from 0.64 to 1.22 μm and the highest distribution density of BCG (0.74 μm grain size) was 2.28 μm⁻³.

Although the electrolyte is often not considered in the elementary steps of electrode modeling, it has been found experimentally that the polarization resistance increases with the increase of electrolyte resistivity.^{34–36} Kenjo et al. have proposed that the electrolyte effect is caused by the locally variable polarization resistance of the electrode.³⁷ However, this is contradictory to our result that lower electrolyte conductivity accompanies better interfacial electrochemical performance. Wang et al. measured the polarization resistance of the LSCF cathode on different ratios of Sm-doped ceria electrolytes and indicated that polarization resistance and the conductivity do not follow a linear relationship in doped ceria because the ORR in the cathode contains several discrete steps.³⁶ This work also provides evidence that in certain cases, the cathode performance could be improved, even with lower ionic conductivity levels for a doped ceria electrolyte.

In a mixed conductor such as LSCF used as a cathode, the cathodic reaction area would be extended to the entire surface, as shown in Figure 7. In the LSCF frame, oxygen is reduced to

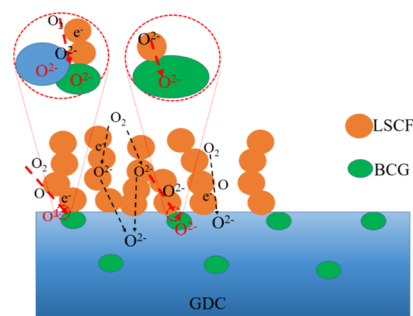


Figure 7. ORR mechanism schematic diagram for the LSCF cathode on the SBCG–GDC electrolyte.

oxygen ion ($O_2 + 4e^- = 2O^{2-}$), followed by oxygen ion incorporation into the GDC electrolyte. In the present work employing LSCF electrodes, the enhanced performance must be attributed to the interface between the LSCF and SBCG–GDC electrolyte. In heterostructured electrolytes, the oxygen incorporation reaction in LSCF and the SBCG–GDC interface would be divided into two sections: (i) the GDC grain and (ii) the BCG grain. In this work, all measurements were conducted in dry air atmosphere (no water), resulting in exclusive oxygen ion conductivity for the BCG phase. However, when we consider that the volume fraction of the BCG phase is only about 6.25% (limited BCG grains on the surface) the properties of BCG by itself could not be responsible for the observed reduction in polarization resistance. It is proposed that there is a synergistic effect of the BCG phase on the ORR between the LSCF electrode and the main electrolyte component GDC. As proposed by Hu et al.,³⁸ the effective oxygen diffusion distance on the LSCF–GDC interface triple phase boundary is about 1.5 μm and the diffusion step is known to dominate the oxygen incorporation reaction. The behavior observed in the present work may be due to the enlarged effective diffusion distance created by the BCG phase in the heterostructured SBCG–GDC electrolyte, which facilitates the oxygen incorporation process. Further work needs to be done to confirm this hypothesis and investigate the effective oxygen diffusion distance in the BCG–GDC electrolyte.

Full Cell Performance and Long-Term Stability. The full cell SOFC performance was evaluated for a SBCG–GDC electrolyte full cell with an LSCF cathode. Figure 8a shows the cell voltage and power density from 500 to 650 °C as a function of current density when humidified hydrogen was used as the fuel and ambient air as the oxidant. The peak power densities at 500, 550, 600, and 650 °C were 0.20, 0.35, 0.53, and 0.70 W cm⁻², respectively. Figure 8b presents long-term stability tests where the full cell was run at a constant voltage of 0.7 V at 600 °C for 100 h and the current density was recorded as a function of time. The current density remained constant at about 0.44 A cm⁻², and there was no observed degradation in the 100 h test. The impedance spectra measured under open-circuit conditions are also displayed in Figure 8b, indicating the SBCG–GDC electrolyte resistance was 0.3 Ω cm², whereas the polarization resistance of the LSCF cathode was 0.44 Ω cm².

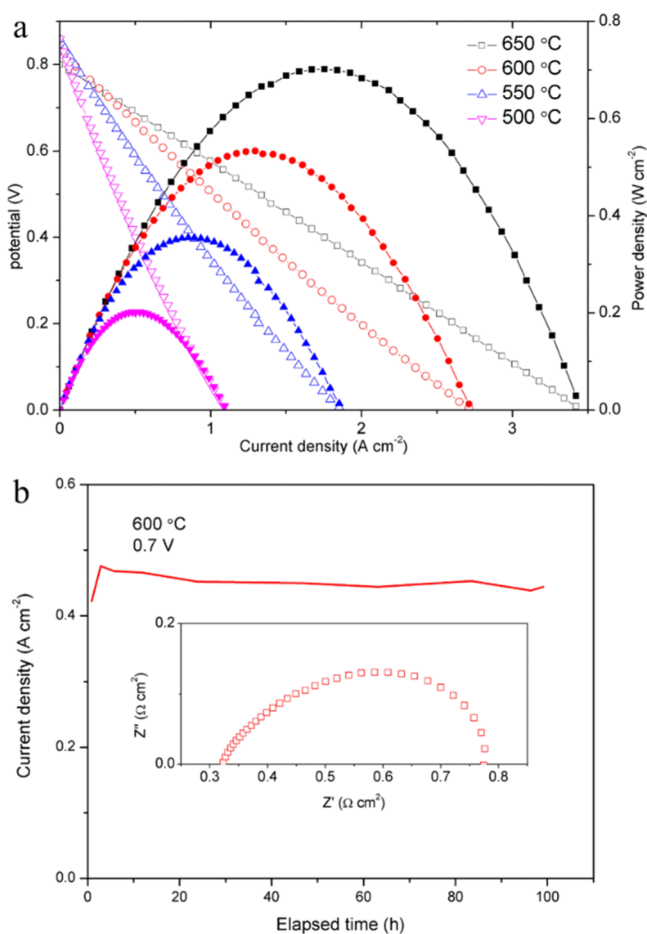


Figure 8. (a) V - I performance of the SBCG-GDC electrolyte full cell with the LSCF cathode and (b) current density with 0.7 V voltage at 600 °C and corresponding ac impedance spectra.

It is known that barium cerate-based electrolytes display poor chemical stability in the presence of acidic gases such as CO_2 in air.^{39,40} In the typical full cell operating conditions, CO_2 reacts with alkaline metals in barium cerates and forms carbonates, as predicted from thermodynamic calculations and widely observed in experiments.⁴¹⁻⁴³ A single cell SOFC

fabricated with BCS electrolytes was shown to react with CO_2 in air, resulting in serious decomposition of the BCS electrolyte in just 24 h under working condition.⁴¹ Therefore, the stability of the BCG phase in the SBCG-GDC heterostructured electrolyte is a very important factor for the SOFC applications. The morphology of the full cell after 100 h of operation is shown in Figure 9. It is clear that the surfaced and cross-sectional microstructure of the SBCG-GDC thin film electrolyte surface exposed to air (the cathode side) retained a fine grain structure. This is in contrast to coarse grains observed on the surface in pure barium cerate electrolytes.⁴¹ The backscatter SEM image and EDX elemental mapping for cells after 100 h of operation were collected and are displayed in Figure 9c. There is no sign of coarsening or phase separation within the electrolyte bulk and the electrolyte morphology of the tested cell appears identical to an unused/pristine cell. The interfaces between cathode/anode and electrolyte are very clear and uniform for all elements. It has been reported that the carbonation process can degrade the perovskite structure, produce defects such as holes on the surface, and finally decrease the electrolyte performance.^{44,45} After 100 h of operation, the Ba element representing the BCG phase appears to be isolated, indicating no significant elemental migration and segregation, which suggests excellent chemical stability of the heterostructured SBCG-GDC electrolyte.

CONCLUSIONS

Barium carbonate was added to ceria electrolytes to improve the electrochemical performance in SOFCs. The addition of 5 or 10 wt % BaCO_3 resulted in a reaction with GDC at 1000 °C for a new BCG phase. In this new BCG-GDC heterostructured electrolyte, the BCG phase was observed to improve the sintering activity of GDC. The BCG-GDC electrolyte was tested using LSCF, LSM, LSC, and Ag as a cathode, resulting in a dramatic reduction in the polarization resistance (for LSCF at 600 and 700 °C, the resistance was reduced from 2.49 and 0.23 to 1.21 and 0.12 $\Omega \text{ cm}^2$) obtained by using pure GDC as an electrolyte. In full cell long-term operation, the SBCG-GDC electrolyte was found to be stable in air atmosphere and no reaction was observed with residual CO_2 . This approach of tailoring the surface reactivity by tailoring the composition and structure of the electrolyte as opposed to electrode materials

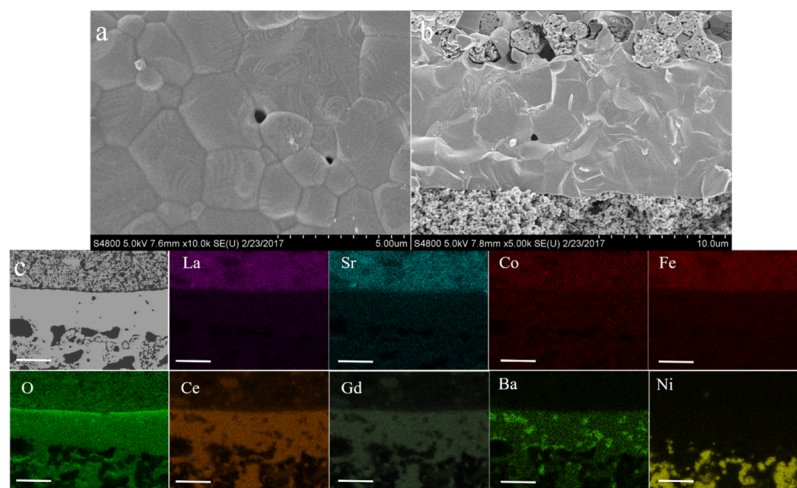


Figure 9. (a) Surface area and (b) cross section of the SBCG-GDC electrolyte after 100 h of operation. (c) Backscatter SEM of full cell cross section after the 100 h test and EDX element mapping in BSE mode for La, Sr, Co, Fe, Ce, Gd, Ba, and Ni elements. Scale bars, 10 μm .

proved to be an effective and novel method to improve fuel cell performance.

METHODS AND MATERIALS

Sample Preparation. ($\text{Gd}_{0.2}\text{Ce}_{0.8}\text{O}_{2-\delta}$) GDC powder (Fuelcell Materials Company Co. Ltd.) was mixed with 5 and 10 wt % barium carbonate followed by ball milling in ethanol for 24 h. Dense cylindrical GDC and BaCO_3 -GDC pellets were prepared by uniaxially pressing these powders followed by sintering at 1500 °C for 5 h. To evaluate the interfacial polarization resistance, symmetric cells with LSCF, LSM, LSC, and Ag (Advanced Materials Company Co. Ltd.) cathodes were fabricated on both sides of the GDC electrolytes. The LSCF, LSM, LSC, and Ag slurries were prepared by mixing the powders with an organic binder (Heraeus Co. Ltd.) and heated at 1000, 1000, 900, and 800 °C for 2 h to form the symmetrical cells.

Full cells were fabricated with the configuration of NiO-GDC anode substrates and SBCG-GDC electrolytes. The anode powders consisting of 60 wt % NiO and 40 wt % GDC were dry pressed at 200 MPa with starch as a pore former. The SBCG-GDC electrolyte layers were deposited on the anode support by the dip-coating process and were then sintered at 1500 °C for 5 h. The LSCF cathode was applied on the electrolytes by the same procedure used in symmetrical cell fabrication.

Sample Characterization. XRD (Rigaku TTR-III) analysis was used to examine the phase of the GDC, BCG, and BaCO_3 at the scan rate of 1° per min. The morphologies of the LSCF, LSM, and LSC electrodes were examined using an SEM (Hitachi S-4800). EDX spectroscopy was measured on the full cell cross section (sealed in synthetic resin and polished by sand papers) by an energy-dispersive spectrometer (Oxford) at the voltage of 20 kV. Thermal gravitation (METTLER TOLEDO) was employed to analyze the barium acetate decomposition process. The sinter curves of GDC and SBCG-GDC were determined by using a dilatometer (NETZSCH DIL402C) at a heating rate of 5 °C/min. The 3D distribution of the BCG particles was reconstructed from the SEM-EDX images, using the two-point correlation function principles developed by Jiao et al.²² Then, the distribution of the diameter of BCG particles was calculated from the 3D reconstructed network of BCG particles, represented by the diameters of the inscribed spheres.

Electrochemical Testing. Impedance spectra were acquired using a Solartron 1287 + 1260 electrochemical workstation with an ac amplitude of 10 mV in the frequency range from 1 MHz to 0.1 Hz using Ag as the current collector and were fitted using Zview software. The performance of the single cell was evaluated using humidified (~3% H_2O) hydrogen as the fuel and ambient air as the oxidant.

ASSOCIATED CONTENT

Supporting Information

The Supporting Information is available free of charge on the ACS Publications website at DOI: 10.1021/acsomega.8b02127.

Morphology of LSCF electrode supported on GDC, SBCG-GDC, and 10BCG-GDC electrolytes; Bode spectra for the EIS test and SEM images for LSC and LSM cathodes supported by GDC and SBCG-GDC electrolytes (PDF)

AUTHOR INFORMATION

Corresponding Authors

*E-mail: taoh@hfut.edu.cn. Phone: +86-551-62901361 (T.H.).

*E-mail: ksbrink@clemson.edu (K.B.).

ORCID

Tao Hong: 0000-0001-9589-4833

Yanxiang Zhang: 0000-0002-8254-5391

Kyle Brinkman: 0000-0002-2219-1253

Author Contributions

The article was written through contributions of all the authors. All the authors have given approval to the final version of the article.

Notes

The authors declare no competing financial interest.

ACKNOWLEDGMENTS

We gratefully acknowledge the financial support from the National Natural Science Foundation of China (51802065), China Postdoctoral Science Foundation (2018M630702), and the Department of Energy, Nuclear Energy Research Program (DOE-NEUP) Project 14-6357, A New Paradigm for Understanding Multi-phase Ceramic Waste Form performance. K.B. was supported in part by an appointment to the National Energy Technology Laboratory Research Participation Program, sponsored by the U.S. Department of Energy and administered by the Oak Ridge Institute for Science and Education.

REFERENCES

- (1) Faber, J.; Geoffroy, C.; Roux, A.; Sylvestre, A.; Abelard, P. A systematic investigation of the dc electrical conductivity of rare-earth doped ceria. *Appl. Phys. A: Solids Surf.* **1989**, *49*, 225–232.
- (2) Eguchi, K.; Setoguchi, T.; Inoue, T.; Arai, H. Electrical properties of ceria-based oxides and their application to solid oxide fuel cells. *Solid State Ionics* **1992**, *52*, 165–172.
- (3) Inaba, H.; Tagawa, H. Ceria-based solid electrolytes. *Solid State Ionics* **1996**, *83*, 1–16.
- (4) Inaba, H.; Sagawa, R.; Hayashi, H.; Kawamura, K. Molecular dynamics simulation of gadolinia-doped ceria. *Solid State Ionics* **1999**, *122*, 95–103.
- (5) Chen, Y.; Chen, Y.; Ding, D.; Ding, Y.; Choi, Y.; Zhang, L.; Yoo, S.; Chen, D.; deGlee, B.; Xu, H.; Zhao, B.; Vardar, G.; Wang, J.; Bluhm, H.; Crumlin, E. J.; Yang, C.; Liu, J.; Yildiz, B.; Liu, M. A robust and active hybrid catalyst for facile oxygen reduction in solid oxide fuel cells. *Energy Environ. Sci.* **2017**, *10*, 964–971.
- (6) Chen, Y.; Choi, Y.; Yoo, S.; Ding, Y.; Yan, R.; Pei, K.; Qu, C.; Zhang, L.; Chang, I.; Zhao, B.; Chen, H.; Chen, Y.; Yang, C.; deGlee, B.; Murphy, R.; Liu, J.; Liu, M. A Highly Efficient Multi-phase Catalyst Dramatically Enhances the Rate of Oxygen Reduction. *Joule* **2018**, *2*, 938–949.
- (7) Chen, Y.; Yoo, S.; Pei, K.; Chen, D.; Zhang, L.; deGlee, B.; Murphy, R.; Zhao, B.; Zhang, Y.; Chen, Y.; Liu, M. An In Situ Formed, Dual-Phase Cathode with a Highly Active Catalyst Coating for Protonic Ceramic Fuel Cells. *Adv. Funct. Mater.* **2018**, *28*, 1704907.
- (8) Liu, D.; WANG, Q.; PENG, K. Preparation and Characterization of Composite Electrolyte Powder $\text{BaCe}_{0.8}\text{Y}_{0.2}\text{O}_{3-\delta}$ - $\text{Ce}_{0.8}\text{Gd}_{0.2}\text{O}_{1.9}$ for Solid Oxide Fuel Cells. *J. Chin. Ceram. Soc.* **2012**, *40*, 752–757.
- (9) Li, B.; Liu, S.; Liu, X.; Qi, S.; Yu, J.; Wang, H.; Su, W. Electrical properties of SDC-BCY composite electrolytes for intermediate temperature solid oxide fuel cell. *Int. J. Hydrogen Energy* **2014**, *39*, 14376–14380.

- (10) Østergård, M. J. L.; Clausen, C.; Bagger, C.; Mogensen, M. Manganite-zirconia composite cathodes for SOFC: Influence of structure and composition. *Electrochim. Acta* **1995**, *40*, 1971–1981.
- (11) Murray, E. P.; Sever, M.; Barnett, S. Electrochemical performance of (La, Sr)(Co, Fe)O₃–(Ce, Gd)O₂ composite cathodes. *Solid State Ionics* **2002**, *148*, 27–34.
- (12) Shao, Z.; Haile, S. M. A high-performance cathode for the next generation of solid-oxide fuel cells. *Nature* **2004**, *431*, 170–173.
- (13) Kim, G.; Wang, S.; Jacobson, A. J.; Reimus, L.; Brodersen, P.; Mims, C. A. Rapid oxygen ion diffusion and surface exchange kinetics in PrBaCo₂O_{5+x} with a perovskite related structure and ordered A cations. *J. Mater. Chem.* **2007**, *17*, 2500–2505.
- (14) Skinner, S.; Kilner, J. Oxygen diffusion and surface exchange in La_{2-x}Sr_xNiO_{4+δ}. *Solid State Ionics* **2000**, *135*, 709–712.
- (15) Hong, T.; Zhao, M.; Brinkman, K.; Chen, F.; Xia, C. Enhanced Oxygen Reduction Activity on Ruddlesden–Popper Phase Decorated La_{0.8}Sr_{0.2}FeO_{3-δ} 3D Heterostructured Cathode for Solid Oxide Fuel Cells. *ACS Appl. Mater. Interfaces* **2017**, *9*, 8659–8668.
- (16) Gao, Z.; Mogni, L. V.; Miller, E. C.; Railsback, J. G.; Barnett, S. A. A perspective on low-temperature solid oxide fuel cells. *Energy Environ. Sci.* **2016**, *9*, 1602–1644.
- (17) Ding, D.; Li, X.; Lai, S. Y.; Gerdes, K.; Liu, M. Enhancing SOFC cathode performance by surface modification through infiltration. *Energy Environ. Sci.* **2014**, *7*, 552–575.
- (18) Jiang, Z.; Xia, C.; Chen, F. Nano-structured composite cathodes for intermediate-temperature solid oxide fuel cells via an infiltration/impregnation technique. *Electrochim. Acta* **2010**, *55*, 3595–3605.
- (19) Sata, N.; Eberman, K.; Eberl, K.; Maier, J. Mesoscopic fast ion conduction in nanometre-scale planar heterostructures. *Nature* **2000**, *408*, 946–949.
- (20) Garcia-Barriocanal, J.; Rivera-Calzada, A.; Varela, M.; Sefrioui, Z.; Iborra, E.; Leon, C.; Pennycook, S. J.; Santamaria, J. Colossal ionic conductivity at interfaces of epitaxial ZrO₂: Y₂O₃/SrTiO₃ heterostructures. *Science* **2008**, *321*, 676–680.
- (21) Maier, J. Nanoionics: ion transport and electrochemical storage in confined systems. *Nat. Mater.* **2005**, *4*, 805–815.
- (22) Jiao, Y.; Stillinger, F. H.; Torquato, S. Modeling heterogeneous materials via two-point correlation functions: basic principles. *Phys. Rev. E - Stat. Nonlinear Soft Matter Phys.* **2007**, *76*, 031110.
- (23) Tomita, A.; Tachi, Y.; Hibino, T. Blocking of Electronic Current through a Ce_{0.9}Gd_{0.1}O_{1.95} Electrolyte Film by Growth of a Thin BaCe_{1-x}Gd_xO₃ Layer. *Electrochem. Solid-State Lett.* **2008**, *11*, B68–B70.
- (24) Sun, W.; Shi, Z.; Qian, J.; Wang, Z.; Liu, W. In-situ formed Ce_{0.8}Sm_{0.2}O_{2-δ}@Ba(Ce, Zr)_{1-x}(Sm, Y)_xO_{3-δ} core/shell electron-blocking layer towards Ce_{0.8}Sm_{0.2}O_{2-δ}-based solid oxide fuel cells with high open circuit voltages. *Nano Energy* **2014**, *8*, 305–311.
- (25) Zha, S.; Xia, C.; Meng, G. Effect of Gd (Sm) doping on properties of ceria electrolyte for solid oxide fuel cells. *J. Power Sources* **2003**, *115*, 44–48.
- (26) Bonanos, N.; Ellis, B.; Knight, K.; Mahmood, M. Ionic conductivity of gadolinium-doped barium cerate perovskites. *Solid State Ionics* **1989**, *35*, 179–188.
- (27) Maffei, N.; Pelletier, L.; McFarlan, A. Performance characteristics of Gd-doped barium cerate-based fuel cells. *J. Power Sources* **2004**, *136*, 24–29.
- (28) Bonano, N.; Ellis, B.; Mahmood, M. Construction and operation of fuel cells based on the solid electrolyte BaCeO₃: Gd. *Solid State Ionics* **1991**, *44*, 305–311.
- (29) Nie, L.; Liu, M.; Zhang, Y.; Liu, M. La_{0.6}Sr_{0.4}Co_{0.2}Fe_{0.8}O_{3-δ} cathodes infiltrated with samarium-doped cerium oxide for solid oxide fuel cells. *J. Power Sources* **2010**, *195*, 4704–4708.
- (30) Hong, T.; Brinkman, K. S.; Xia, C. Barium Carbonate Nanoparticles as Synergistic Catalysts for the Oxygen Reduction Reaction on La_{0.6}Sr_{0.4}Co_{0.2}Fe_{0.8}O_{3-δ} Solid-Oxide Fuel Cell Cathodes. *ChemElectroChem* **2016**, *3*, 805–813.
- (31) Baumann, F. S.; Fleig, J.; Konuma, M.; Starke, U.; Habermeier, H.-U.; Maier, J. Strong performance improvement of (La, Sr)(Co, Fe)O_{3-δ} SOFC cathodes by electrochemical activation. *J. Electrochem. Soc.* **2005**, *152*, A2074.
- (32) Baumann, F.; Fleig, J.; Habermeier, H.; Maier, J. Impedance spectroscopic study on well-defined (La, Sr)(Co, Fe) O_{3-δ} model electrodes. *Solid State Ionics* **2006**, *177*, 1071–1081.
- (33) Lee, J.-W.; Liu, Z.; Yang, L.; Abernathy, H.; Choi, S.-H.; Kim, H.-E.; Liu, M. Preparation of dense and uniform La_{0.6}Sr_{0.4}Co_{0.2}Fe_{0.8}O_{3-δ} (LSCF) films for fundamental studies of SOFC cathodes. *J. Power Sources* **2009**, *190*, 307–310.
- (34) Liu, M.; Wu, Z. Significance of interfaces in solid-state cells with porous electrodes of mixed ionic–electronic conductors. *Solid State Ionics* **1998**, *107*, 105–110.
- (35) Uchida, H.; Yoshida, M.; Watanabe, M. Effect of ionic conductivity of zirconia electrolytes on the polarization behavior of various cathodes in solid fuel cells. *J. Electrochem. Soc.* **1999**, *146*, 1.
- (36) Wang, Y.; Zhang, L.; Chen, F.; Xia, C. Effects of doped ceria conductivity on the performance of La_{0.6}Sr_{0.4}Co_{0.2}Fe_{0.8}O_{3-δ} cathode for solid oxide fuel cell. *Int. J. Hydrogen Energy* **2012**, *37*, 8582–8591.
- (37) Kenjo, T.; Kanehira, Y. Influence of the local variation of the polarization resistance on SOFC cathodes. *Solid State Ionics* **2002**, *148*, 1–14.
- (38) Hu, B.; Wang, Y.; Xia, C. Oxygen incorporation at the three-phase boundary of LSCF–SDC composite. *J. Power Sources* **2014**, *269*, 180–188.
- (39) Zuo, C.; Zha, S.; Liu, M.; Hatano, M.; Uchiyama, M. Ba(Zr_{0.1}Ce_{0.7}Y_{0.2})O_{3-δ} as an Electrolyte for Low-Temperature Solid-Oxide Fuel Cells. *Adv. Mater.* **2006**, *18*, 3318–3320.
- (40) Zuo, C.; Dorris, S. E.; Balachandran, U.; Liu, M. Effect of Zr-doping on the chemical stability and hydrogen permeation of the Ni-BaCe_{0.8}Y_{0.2}O_{3-δ} mixed protonic-electronic conductor. *Chem. Mater.* **2006**, *18*, 4647–4650.
- (41) Wang, Y.; Wang, H.; Liu, T.; Chen, F.; Xia, C. Improving the chemical stability of BaCe_{0.8}Sm_{0.2}O_{3-δ} electrolyte by Cl doping for proton-conducting solid oxide fuel cell. *Electrochem. Commun.* **2013**, *28*, 87–90.
- (42) Kreuer, K. D. Aspects of the formation and mobility of protonic charge carriers and the stability of perovskite-type oxides. *Solid State Ionics* **1999**, *125*, 285–302.
- (43) Zakowsky, N.; Williamson, S.; Irvine, J. Elaboration of CO₂ tolerance limits of BaCe_{0.9}Y_{0.1}O_{3-δ} electrolytes for fuel cells and other applications. *Solid State Ionics* **2005**, *176*, 3019–3026.
- (44) Su, F.; Xia, C.; Peng, R. Novel fluoride-doped barium cerate applied as stable electrolyte in proton conducting solid oxide fuel cells. *J. Eur. Ceram. Soc.* **2015**, *35*, 3553–3558.
- (45) Hirabayashi, D.; Tomita, A.; Hibino, T.; Nagao, M.; Sano, M. Design of a Reduction-Resistant Ce_{0.8}Sm_{0.2}O_{1.9} Electrolyte Through Growth of a Thin BaCe_{1-x}Sm_xO_{3-δ} Layer over Electrolyte Surface. *Electrochem. Solid State Lett.* **2004**, *7*, A318.